

# Influence of a cyclic and dynamic loading history on dynamic properties of dry sand, part II: cyclic axial preloading

T. Wichtmann <sup>i)</sup>, Th. Triantafyllidis

*Institute of Soil Mechanics and Foundation Engineering, Ruhr-University Bochum,  
Universitätsstrasse 150, 44801 Bochum, Germany*

---

## Abstract

Initial fabric of a soil induced by its cyclic strain history is an important parameter among others like void ratio, state of stress and amplitude concerning the further accumulation of deformations under cyclic loading. It is of high importance to determine methods in order to estimate the initial fabric of the grain skeleton or the cyclic loading history of the soil. An attempt is made in this paper to correlate small strain stiffness of non-cohesive soil with its cyclic loading history. For this purpose several cyclic triaxial tests with specimens subjected to cyclic axial loading were performed and changes of small strain soil properties due to this cyclic loading were studied. All these tests showed only moderate changes of small strain stiffnesses independently of the different boundary conditions. Thus, a correlation between fabric or strain history and small strain stiffnesses seems not to be possible.

*Key words:* Cyclic triaxial tests on dry sand; fabric; wave velocities; dynamic soil properties; small strain stiffness; shear modulus; damping ratio; resonant column tests

---

## 1 Introduction

The accumulation of deformation of sand due to drained cyclic loading is not only affected by the void ratio, average state of stress and amplitude of cyclic loading. As demonstrated in [1] the cyclic loading history of the soil induced e.g. by seismic vibrations or sedimentation and erosion processes plays also an important role. It is expected that during this cyclic loading history the fabric of the grain skeleton is changed. Due to re-orientation of particles the soil gains a more stable fabric with a lower potential for further accumulation of deformation under cyclic loading (called also frustration). For the purpose of estimation of the accumulative deformations under further cyclic loading the initial condition of fabric or the cyclic loading history, respectively have to be determined. Since the fabric of a soil can hardly be determined by direct measurements indirect methods have to be used. Such an indirect method is the measurement of small strain soil properties (compression and shear wave velocities and the corresponding small strain stiffnesses). It is assumed that a change of fabric leads to changes of the measurable small strain soil properties. In this case the actual

fabric of a soil or its cyclic loading history respectively could be correlated in a certain way with its small strain soil properties. This method would be applicable in situ since small strain soil properties can be determined by means of seismic or dynamic measurements in the field.

In [1] a review of prior scientific work is given as well as some physical background explaining reasons for an increase of small strain stiffnesses due to a cyclic strain history. In the following a loading history with stress controlled cycles is called "preloading", a history with strain controlled cycles is called "prestraining".

It can be assumed that the polarization of preloading and the polarization of the small strain wave whose propagation velocity is measured could be of importance. It was thought to be promising to measure the development of the compression wave velocity with vertical propagation direction during cyclic axial loading because such compression waves are polarized in the vertical direction. This approach was studied in the test series presented in the next chapters, where the development of small strain soil properties of dry sand specimens in cyclic triaxial tests under cyclic axial loading was studied. Different average states of stress, amplitudes of cyclic loading, relative densities and sands were tested.

---

<sup>i)</sup>Corresponding author. Tel.: 0(49)234/3226080; Fax: 0(49)234/3214150

Similarly the measurement of shear wave velocities and the corresponding small strain shear moduli would be interesting in the case of shear strains generated by cyclic torsional prestraining. In this case the cyclic prestraining and the shear wave generated for the measurement of small strain properties are polarized in the same direction. This approach was followed in the test series with cyclic and dynamic torsional prestraining described in [1].

## 2 Test material

The tests documented in this paper were performed on two different sands, one fine sand and one medium sand. The grain size distribution curves of the used sands are shown in Fig. 6 in [1]. The medium sand used in the studies presented herein is medium sand 2. In [1] another medium sand (medium sand 1) was used in addition to medium sand 2 in some of the tests and in order to keep an uniform designation these names are maintained in this paper. Table 1 in [1] summarizes the characteristic parameters of the grain distribution curves as well as the minimum and maximum densities of the respective sand material.

## 3 Test equipment and analysis

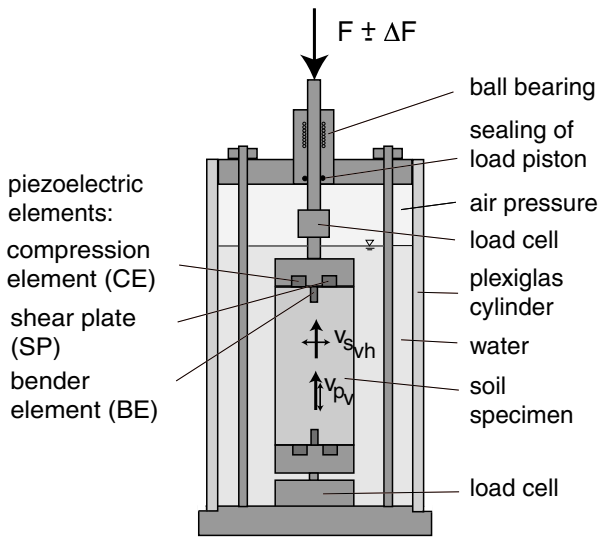


Fig. 1: Scheme of the triaxial cell used in the cyclic triaxial tests

The cyclic triaxial tests were performed in a triaxial cell whose specimen end plates are equipped with pairs of piezoelectric ceramic elements. A scheme of the used cell can be found in Fig. 1. Into the specimen end plates piezoelectric elements of three different types are integrated. A photo of the end plates with the piezoelectric elements can be found in Fig. 2. The so called "compression element" (abbreviated as CE)

generates a deformation in axial direction when an electrical voltage is applied. Thus, a compression wave  $v_{p,v}$  is generated, which propagates in axial direction of the specimen. "Bender Element" (abbreviated as BE) penetrates into the specimen and sends out a shear wave  $v_{s,vh}$  due to the generated bend under an applied voltage. This shear wave propagates in vertical direction and is polarized in horizontal direction. The "Shear Plate" element (abbreviated as SP) is completely integrated into the specimen end plates and is subjected to shear deformations when a voltage is applied. Shear Plates generate the same shear wave as bender elements with the difference that the shear plate elements do not penetrate into the specimen.



Fig. 2: Photo of piezoelectric elements in the lower specimen end plate

The triaxial cell is equipped with two load cells which are waterproof and mounted in the pressure cell. One load cell is integrated into the load piston and thus fixed directly above the specimen, the other is mounted below the lower specimen end plate. Thus, the vertical forces applied to the specimen are measured directly in the pressure cell and a possible falsification of the measured values of vertical force due to friction in the sealing between the load piston and the triaxial cell is avoided. The load piston is guided in a ball bearing and below this bearing a sealing with very low friction is located. The plexiglas cylinder of the triaxial cell sustains cell pressures up to 1000 kPa. In order to apply the cell pressure water is filled into the cell until the upper specimen end plate is completely submerged. The cell pressure is applied on the air cushion remaining in the upper part of the triaxial cell and is regulated by a pressure controller. The vertical force is applied by a pneumatic loading system. The desired value of force is prescribed by a function generator. This target value is transferred to a controller card which compares the target value with the value of force actually measured at the upper load cell in the triaxial cell. If both values

differ the pneumatic ventil receives a signal to regulate the air pressure applied to the pneumatic cylinder which is mounted on the traverse of the testing frame. The pneumatic cylinder applies the vertical force onto the load piston of the triaxial cell. If a cyclic vertical loading should be applied to the specimen the average value of vertical force is specified by the offset function of the function generator and a cyclic amplitude is superimposed by its amplitude function.

All tests in the series described later were conducted on dry sands because the velocity of compression waves propagating through the grain skeleton should be measured. In the case of water saturated specimens this is difficult because the part of the compression wave propagating through the pore water is faster than that propagating through the skeleton and thus the arrival of the latter one is masked by the signal of the former one. Volume changes were measured by means of six non-contact local displacement transducers, because measurements with the pore water were not possible. These transducers were evenly distributed over the surface of the specimen in three different heights and three vertical axes. Aluminium plates were glued on the membrane of the specimen. The displacement transducers were mounted in some distance from these targets. Relative displacements of transducer and target could be measured and thus local lateral deformation values were obtained. With these values and the vertical displacement measured by means of a displacement transducer mounted on the load piston outside the triaxial cell the volume change of the specimen could be calculated.

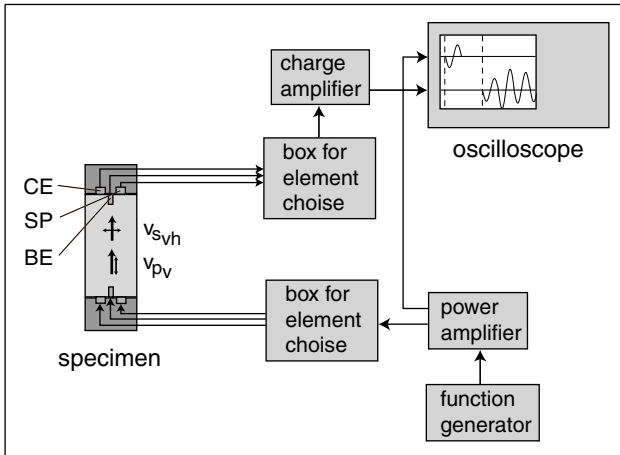


Fig. 3: Measurement technique used to determine wave propagation velocities

A scheme of the measurement technique used to determine the wave velocities is shown in Fig. 3. A single sinusoidal voltage impulse with a high frequency is generated by a function generator. This impulse is amplified by a power amplifier. From this amplifier the signal

is conducted towards an oscilloscope and towards a box at which the element can be chosen on which the signal should be applied. Depending on the adjustment of this box the signal is applied to compression element, bender element or shear plate in the lower specimen end plate. The voltage impulse generates a deformation of the elements which results in the generation of the corresponding wave in the specimen. The arrival of the wave at the piezoelectric elements in the upper end plate of the specimen causes a deformation of these elements and this results in an electrical voltage. This electrical voltage is conducted via a box for the chosen element towards a charge amplifier. The amplified signal is forwarded to the oscilloscope. Typical source and receiver signals are presented in Fig. 12. The arrival times of the source and receiver signals can be determined at the oscilloscope and thus the time difference between these two arrivals  $t_m$  can be calculated. In order to calculate the travel time  $t_t$  of a wave in the specimen the measured time difference has to be corrected by the time the signals are delayed in cables, amplifiers and measurement devices:

$$t_t = t_m - t_c \quad (1)$$

These correction times  $t_c$  were determined in a calibration done with aluminium rods of known length, density and elastic properties. The wave velocity  $v$  can be determined as the quotient of travel length and travel time:

$$v = \frac{l_t}{t_t} \quad (2)$$

In the case of compression element and shear plate the travel length is identical with the specimen height. In the case of bender element the distance between the tips of the elements is the approximation of the travel length. From the measured compression and shear wave velocities the corresponding small strain stiffnesses could be calculated with the actual density  $\rho$ .

$$E_{s0} = v_{p,v}^2 \rho \quad (3)$$

$$G_0 = v_{s,vh}^2 \rho \quad (4)$$

where  $G_0$  is the small strain shear modulus corresponding to the shear wave velocity  $v_{s,vh}$  with a vertical propagation direction and a horizontal polarization.  $E_{s0}$  is the small strain constrained elastic modulus corresponding to the compression wave velocity  $v_{p,v}$  with a vertical propagation and polarization direction. Since only compression waves of type  $v_{p,v}$  and shear waves of type  $v_{s,vh}$  could be measured in this triaxial cell these wave velocities are referenced as  $v_p$  and  $v_s$  in the following.

## 4 Specimen preparation

Specimens with a diameter of 10 cm and a height of 20 cm were prepared directly in the testing device. Dry sand was pluviated out of a funnel through air into half-cylinder moulds. The distance between the sand surface and the funnel was kept constant during pluviation. Different initial densities were achieved by varying funnel diameter and fall height of the sand. After the pluviation the cap of the triaxial cell with the load piston and the upper specimen end plate was mounted. The load piston with the upper specimen end plate was let down onto the specimen. After sealing of the specimen a vacuum of 50 kPa was applied to the grain skeleton and the moulds were removed. The geometry of the specimen was measured and the non-contact lateral displacement transducers were mounted. Thereafter the plexiglas cylinder was placed and fixed and water was filled into the cell. While the vacuum was reduced in steps of 10 kPa the cell pressure was increased in the same steps so that the resulting effective confining pressure was kept constant. After the vacuum was reduced completely the desired confining pressure was applied. Next the specimen was subjected to the desired vertical force by means of the pneumatic loading system. The deformation of the specimen during the application of confining pressure and vertical force was measured.

## 5 Tests on the dependence of $G_0$ and $E_{s0}$ on void ratio and state of stress

In order to determine the dependence of small strain stiffnesses on void ratio and stress an corresponding test series was conducted before the test series with cyclic loading. In order to have the opportunity to compare the results of these tests with the experimental data obtained from a similar test series with the resonant column device described in [1] isotropic stress conditions were chosen within this test series. All tests were performed on medium sand 2. Specimens with different initial densities were prepared. An isotropic confining pressure of  $p = \sigma_1 = \sigma_3 = 50$  kPa was applied. The wave velocities  $v_p$  and  $v_s$  were measured. After that the confining pressure was increased to 100 kPa and the small strain properties were determined again. In this way the confining pressure was increased over 200 kPa and 400 kPa towards 800 kPa. Between the increase of confining pressure and the following measurement of wave velocities in this pressure step it was waited two hours in order to consider aging effects mentioned in [1]. Densifications of specimens due to the increase of confining pressure were documented. From the measured wave velocities and the known densities of the specimens small strain shear modulus  $G_0$  and small strain constrained elastic modulus  $E_{s0}$  could be calculated.

In Fig. 4a) the values of  $E_{s0}$  are presented as a func-

tion of void ratio and confining pressure. Values measured at the same confining pressure are marked with the same grayscale. For a constant confining pressure  $E_{s0}$  decreased with increasing void ratio. From Fig. 4b) one can see the increase of  $E_{s0}$  with increasing confining pressure in four presented tests with different initial densities. Approximately linear curves were obtained in a diagram with double logarithmic scale. Similar tendencies resulted from the measured small strain shear moduli  $G_0$ . In the case of  $G_0$  data from the bender elements were available as well as data from the shear plates. In Fig. 4c) the values measured by bender elements are marked as squares while values obtained from shear plates are presented as circles. It can be seen that there was a good agreement between the values obtained from the two different element pairs. For reasons of clearness in Fig. 4d) only data obtained from measurements with shear plates is presented. The curves obtained in this diagram with double logarithmic scale were nearly linear too.

Functions of the type of equation (8) in [1] were fitted to the experimental data. The following function was determined in the case of small strain constrained elastic modulus:

$$E_{s0} = 1.82 F_{E_{s0}}(e) p_a^{1-2 \cdot 0.20} \sigma_a^{0.20} \sigma_p^{0.20} \quad (5)$$

with the void ratio function

$$F_{E_{s0}}(e) = \frac{(2.36 - e)^2}{1 + e} \quad (6)$$

In the case of small strain shear modulus one obtained:

$$G_0 = 2.84 F_{G_0}(e) p_a^{1-2 \cdot 0.20} \sigma_a^{0.20} \sigma_p^{0.20} \quad (7)$$

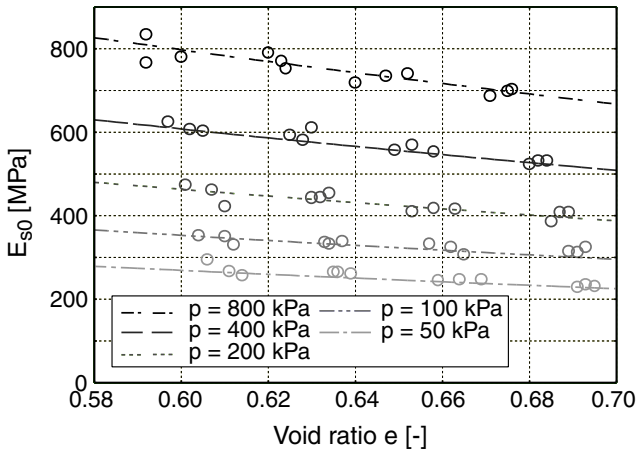
with

$$F_{G_0}(e) = \frac{(1.48 - e)^2}{1 + e} \quad (8)$$

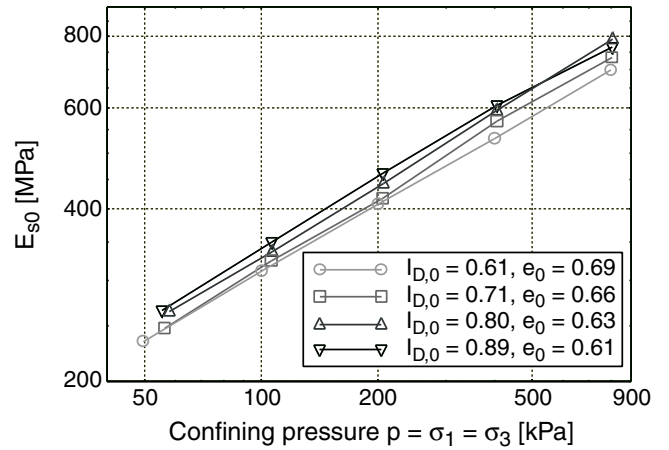
Values calculated with equations (5) and (7) are shown as dashed lines in Figs. 4a) and 4c), respectively. A good agreement between measured and calculated data could be stated. From equations (5) and (7) it could be concluded that the exponent  $n$  was equal for  $E_{s0}$  and  $G_0$ . The reduction of small strain shear modulus with increasing void ratio was somewhat faster in the case of  $G_0$  in comparison with  $E_{s0}$ . This leads to a lower value of the constant  $a$  in the void ratio function and thus the factors  $A$  were different too. For the definition of parameters  $a$  and  $A$  see equation (8) in [1].

Fig. 5 compares the values of small strain shear moduli measured in this test series with data obtained from similar resonant column tests. The values of  $G_0$  are presented in dependence on void ratio and confining pressure. In [1] the following function was fitted

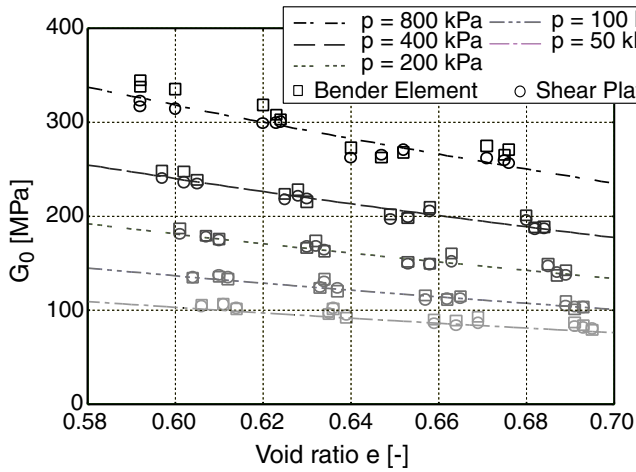
a) Dependence of  $E_{s0}$  on void ratio



b) Dependence of  $E_{s0}$  on isotropic confining pressure



c) Dependence of  $G_0$  on void ratio



d) Dependence of  $G_0$  on isotropic confining pressure

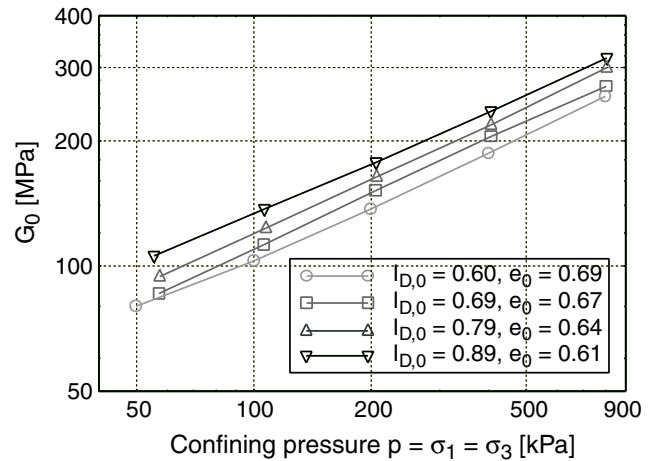


Fig. 4: Dependence of small strain stiffnesses on void ratio and isotropic confining pressure

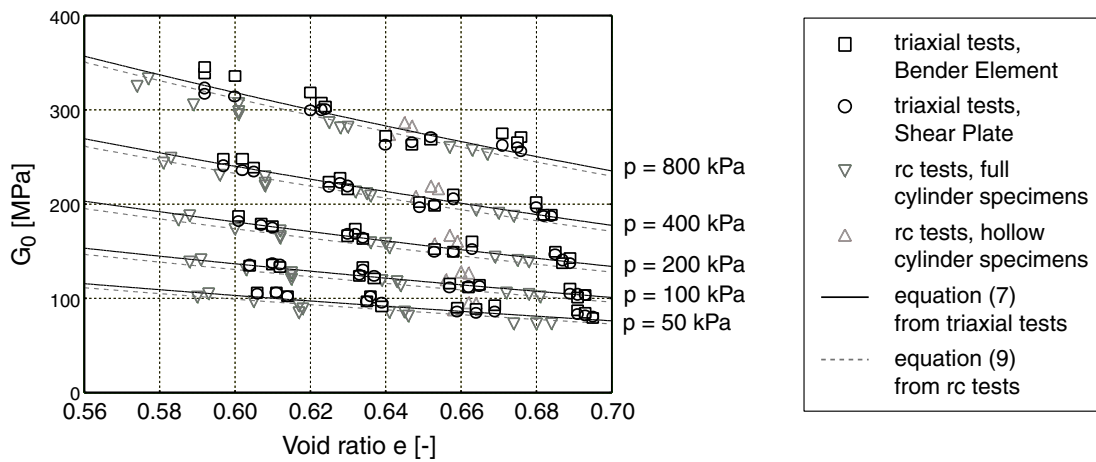


Fig. 5: Comparison of small strain shear moduli  $G_0$  determined in resonant column tests and triaxial tests with measurement of wave propagation velocities

to the experimental data of small strain shear modulus obtained from the resonant column tests:

$$G_0 = 2.75 \frac{(1.46 - e)^2}{1 + e} p_a^{1-2 \cdot 0.21} \sigma_a^{0.21} \sigma_p^{0.21} \quad (9)$$

Data calculated from equations (7) and (8) is shown as black solid lines in Fig. 5. Values calculated from equation (9) are added as dashed gray lines. It can be seen from Fig. 5 and the determined equations (7), (8) and (9) that the data obtained from the two different devices agreed well. The values of small strain shear modulus obtained by the measurement of wave propagation velocities in the triaxial cell were slightly higher than the corresponding values obtained from resonant column tests on full cylinder specimens. This difference could be calculated from equations (7), (8) and (9). It can be stated that the difference did not clearly depend on void ratio or confining pressure but was approximately constant. It is thought that the higher values determined with the piezoelectric elements are due to lower shear strains generated in these measurements in comparison with shear strains used during the determination of  $G_0$  in a resonant column test. Since in resonant column tests measured values of  $G_0$  of hollow cylinder specimens were slightly higher than those measured with full cylinder specimens (see Fig. 5), the different distribution of shear strains over the cross section of the specimens might be another cause for the slight differences between the two test devices. However, since two completely different methods of determination of small strain soil properties were compared the deviation of the measured data seems to be more than satisfactory.

## 6 Cyclic triaxial tests

### 6.1 Testing procedure

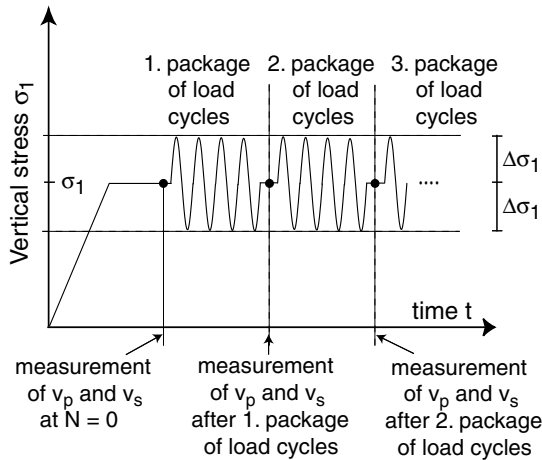


Fig. 6: Testing procedure in the cyclic triaxial tests with measurement of wave propagation velocities

Fig. 6 describes the procedure of this test series. Specimens were prepared in the way described in chapter 4. From the desired values of mean pressure  $p$  and deviatoric stress component  $q$  the needed lateral stress  $\sigma_3$  and vertical stress  $\sigma_1$  were calculated. After this average state of stress was applied and deformations due to secondary compression were abated the wave velocities were measured for the first time. These values correspond to the non-preloaded specimen ( $N = 0$ ). After this measurement the first package of sinusoidal load cycles with an amplitude of  $\Delta\sigma_1$  was applied to the specimen. The number of generated cycles could be specified at the function generator. After the application of each package of cycles the vertical stress returned to the average value  $\sigma_1$  and this value was held constant until the next package of cycles started. After the specimen was subjected to the first package of cycles the wave velocities were measured again. The same procedure followed for the next package of cycles and was repeated several times with increasing number of cycles in the single packages.

After each package of cycles the accumulated deformations of the specimen were documented. Furthermore during the first five cycles of each package the values of all displacement, pressure and force transducers were continuously recorded in order to control the vertical stress amplitude  $\Delta\sigma_1$  and calculate the amplitudes of volumetric strain  $\Delta\varepsilon_{vol}$  and vertical strain  $\Delta\varepsilon_1$ . From volumetric and vertical strain amplitudes the shear strain amplitude  $\gamma$  could be calculated by means of equation (10).

$$\gamma = \Delta\varepsilon_1 - \Delta\varepsilon_3 = \frac{1}{2} (3\Delta\varepsilon_1 - \Delta\varepsilon_{vol}) \quad (10)$$

### 6.2 Testing program

In this test series the average state of stress ( $p, q$ ), the initial relative density  $I_{D,0}$ , the amplitude of cyclic loading  $\Delta\sigma_1$  and the sand was varied. Table 1 summarizes the testing program and contains also the obtained strain amplitudes  $\Delta\varepsilon_1$ ,  $\Delta\varepsilon_{vol}$  and  $\gamma$ . In all performed tests 100,000 load cycles with a frequency of 1 Hz were applied to the specimens. The only exception is test No 4 where the vertical deformations were large enough to cause some of the local non-contact displacement transducers to be out of their measurement range.

### 6.3 Test results

Five tests (No's 1,2,3,4 and 5) were conducted on medium sand 2 in order to study different average states of stress ( $p, q$ ). The tests were chosen in such a way that three of these tests were performed with identical mean pressure  $p$  but different values of  $q$  and also

Test No	Sand	$p$ [kPa]	$q$ [kPa]	$\Delta\sigma_1$ [kPa]	$I_{D,0}$ [-]	$I_{D,S}$ [-]	$\Delta\varepsilon_1$ [%]	$\Delta\varepsilon_{vol}$ [%]	$\gamma$ [%]
1	MS2	200	100	60	0.57	0.59	0.030	0.018	0.035
2	MS2	200	200	60	0.59	0.61	0.028	0.017	0.033
3	MS2	200	150	60	0.58	0.61	0.029	0.018	0.035
4	MS2	100	100	60	0.58	0.60	0.042	0.021	0.048
5	MS2	150	100	60	0.59	0.61	0.035	0.022	0.041
6	MS2	200	150	60	0.29	0.33	0.030	0.017	0.037
7	MS2	200	150	60	1.03	1.05	0.023	0.017	0.025
8	MS2	200	150	30	0.61	0.63	0.015	0.010	0.017
9	MS2	200	150	90	0.60	0.63	0.043	0.026	0.052
10	FS	200	150	60	0.50	0.53	0.023	0.014	0.028

Table 1: Testing program of cyclic triaxial tests with measurement of wave velocities and resulting strain amplitudes

three tests had the same deviatoric stress  $q$  but different mean pressures  $p$  (see Fig. 7). Mean pressures between 100 kPa and 200 kPa were tested, the deviatoric stress component was also chosen in the range between 100 kPa and 200 kPa. The amplitude of cyclic loading was kept constant at  $\Delta\sigma_1 = 60$  kPa. Relative densities after specimen preparation lay in the range  $0.57 \leq I_{D,0} \leq 0.59$ . The relative densities after the application of the average state of stress are named  $I_{D,S}$  and can be found in Table 1. Fig. 7 shows the average states of stress chosen in these five tests and the maximum and minimum values of  $p$  and  $q$  resulting from cycles with  $\Delta\sigma_1$ . The presented critical state line (CSL) was drawn with a critical angle of friction of  $\varphi_c = 31.2^\circ$ . This value was determined as a mean value of the slopes of pluviated cones observed in ten tests on medium sand 2. The peak angle of friction  $\varphi_p = 36.8^\circ$  also presented in Fig. 7 was obtained from drained static triaxial tests on the same sand with an initial relative density of  $I_D = 0.65$ .

Fig. 8a) presents the accumulated vertical strain as a function of the number of applied load cycles  $N$ . A reduction of specimen height results in positive values of  $\varepsilon_1^{acc}$ . The  $N$ -axis is scaled logarithmically. It has to be stated that the influence of mean pressure  $p$  was much more significant than the influence of the deviatoric stress component  $q$ . We consider the three tests with identical  $q$  (No's 4, 5 and 1) but different mean pressures  $p$ . The lower the mean pressure  $p$  the larger was the accumulated vertical strain. This can partly be attributed to the higher shear strain amplitudes  $\gamma$  generated at smaller mean pressures but identical stress amplitudes (see Table 1). In the case of the lowest tested mean pressure the deformations due to 50,000 load cycles were quite high reaching 3.2 %. Concerning the influence of the deviatoric pressure we take into account the tests No's 1, 3 and 2 with identical mean

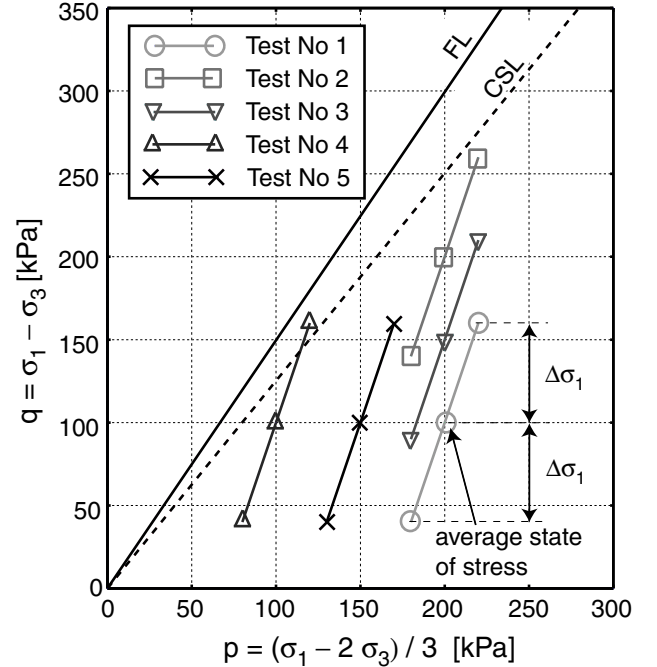


Fig. 7: Average state of stress and cyclic stress path in the cyclic triaxial tests with varying average state of stress. CSL = critical state line ( $\varphi_c = 31.2^\circ$ ), FL = failure line ( $\varphi_p = 36.8^\circ$ )

pressure but with different values of  $q$ . Similar shear strain amplitudes  $\gamma$  were generated due to the cyclic stress amplitude as can be seen in Table 1. It has to be stated that the higher the deviatoric stress  $q$  was the higher was the accumulated vertical strain. However the differences of these three tests concerning the accumulated vertical strain were only moderate.

Fig. 8b) shows the corresponding curves of accumulated volumetric strain. A reduction of volume results

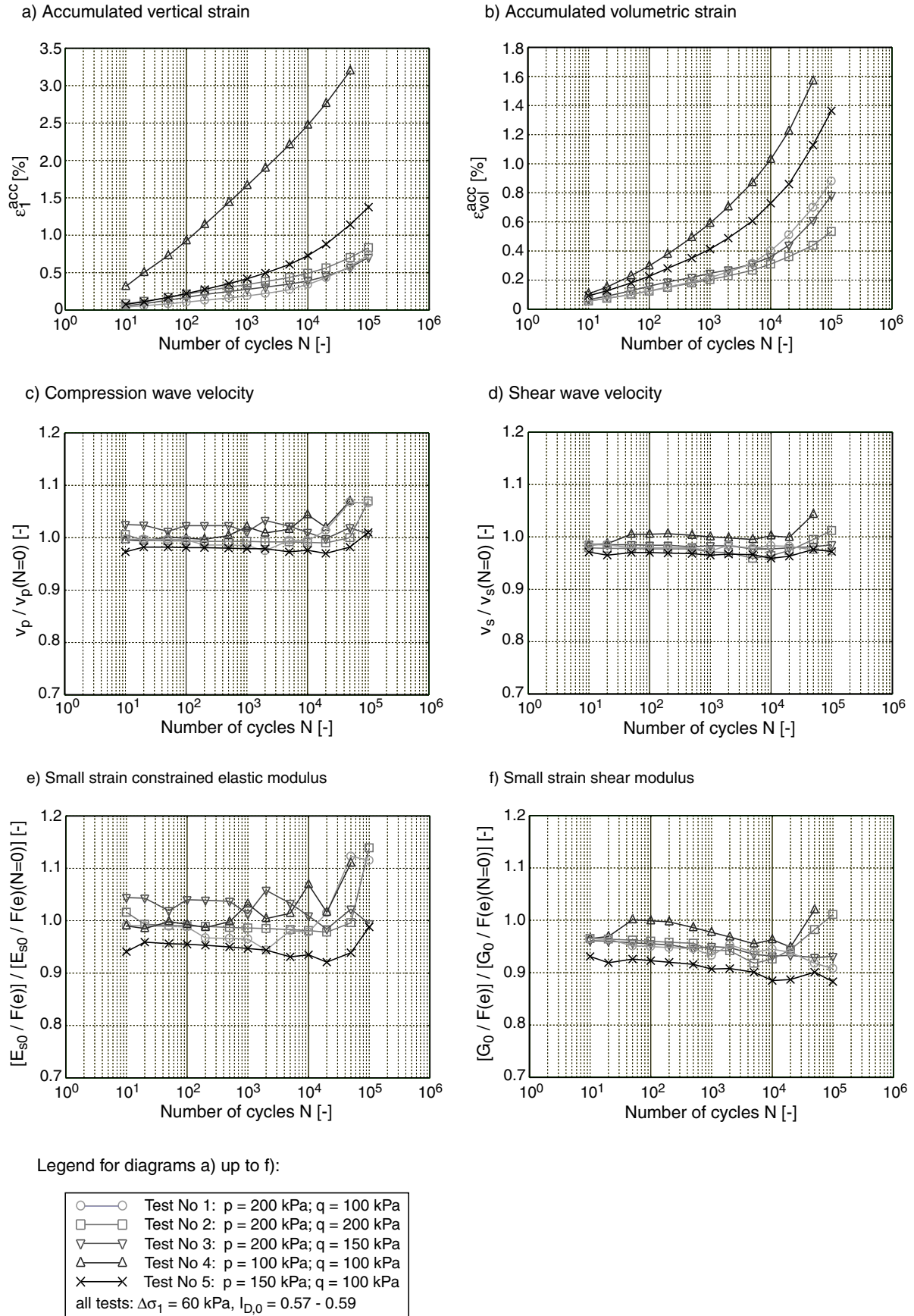


Fig. 8: Results of cyclic triaxial tests with variation of average state of stress

in positive values of  $\varepsilon_{\text{vol}}^{\text{acc}}$ . The dependence of the accumulated volumetric strain on the mean pressure was similar to that observed in the diagram of the accumulated vertical strain. The lower the mean pressure was the larger was the accumulated volumetric strain. Concerning the influence of deviatoric stress component  $q$  an opposite behavior was observed as in the case of the accumulation of vertical strain. A smaller value of  $q$  resulted in a larger accumulation of  $\varepsilon_{\text{vol}}$ . As in the case of  $\varepsilon_1^{\text{acc}}$  the influence of mean pressure  $p$  was larger than that of deviatoric stress component  $q$ .

It has to be mentioned here that the accumulated strains presented in Figs. 8a) and 8b) and the following figures do not contain the deformations during the first cycle of loading since the first quarter of this cycle results in deformations that correspond to first loading and are not considered as accumulated deformation due to cyclic loading. The deformations in the three following quarters of this first cycle are negligible in comparison with the deformations accumulated during the huge number of following cycles. A comparison of the measured accumulated deformations in the test series presented herein with data of a test series performed in another cyclic triaxial device using the same boundary conditions but measuring volume changes by means of the squeezed out pore water showed satisfiable agreement of measured curves.

Fig. 8c) presents the development of compression wave velocity  $v_p$  during cyclic loading. The measured values are normalized with the values measured prior to the first package of cycles. It can be stated that in all performed tests  $v_p$  stayed nearly constant over 100,000 load cycles. During the first cycles the compression wave velocity was slightly changed (increased or decreased) but this change did not exceed 5 % and no clear dependence of this change on mean pressure or the deviatoric stress component could be determined. Some of the curves showed a moderate increase of  $v_p$  after 20,000 load cycles but even after 100,000 load cycles the compression wave velocity of none of the specimens was increased more than 8 % in comparison with the values determined before cyclic loading.

Similar results were obtained from the measurements of shear wave velocity which are shown in Fig. 8d). Shear wave velocity was slightly reduced in all of the tests during the first 10 load cycles. During the following cycles  $v_s$  stayed nearly constant and only after 20,000 load cycles a small increase of  $v_s$  could be observed. The highest increase of shear wave velocity was measured in the test with the lowest mean pressure but did not exceed 5 % after 50,000 load cycles compared with the values before cyclic loading. In contradiction to the diagrams of small strain stiffnesses described below the reduction of void ratio during cyclic loading was not taken into account in the diagrams of the wave

propagation velocities. A reduction of void ratio leads to an increase of the wave velocities.

In Fig. 8e) the development of small strain constrained elastic modulus  $E_{s0}$  is presented. In order to eliminate the influence of the decreasing void ratio during cyclic loading, the measured values of  $E_{s0}$  were divided by the void ratio function (6). Although this function was determined in tests with isotropic states of stress it will be demonstrated later that equation (6) is also applicable in the case of  $q > 0$ . These values  $E_{s0}/F_{E_{s0}}(e)$  measured after  $N$  applied load cycles were normalized with the corresponding values before the first package of cycles. The tendencies were the same as described in the discussion of Fig. 8c). Only moderate increases of stiffness could be determined at cycles  $N \geq 20,000$ . Stiffness increases did not exceed 14 % after 100,000 applied load cycles.

In Fig. 8f) the development of small strain shear modulus is shown. As in the case of small strain constrained elastic modulus the values of  $G_0$  were divided with the void ratio function (8) and normalized in the same way described above. The tendencies of the curves presented in Fig. 8f) were the same as discussed in the case of shear wave velocity. The shear modulus was reduced during the first 10 load cycles. This agrees with observations made in resonant column tests with dynamic prestraining of specimens (see [1]).  $G_0$  tended to decrease in the following cycles in most of the tests but after 20,000 cycles some of the tests showed a stagnation or an increase in small strain shear stiffness. However, these changes were small and almost negligible. A similar slight decrease of small strain shear modulus was observed during dynamic prestraining of hollow cylinder specimens of medium sand 2 in the resonant column device as presented in [1].

Two additional tests (No's 6 and 7) were performed on medium sand 2 in order to study a possible influence of initial density on the development of small strain properties during cyclic loading. These tests were performed with an average state of stress lying on the  $K_0$ -line ( $p = 200$  kPa,  $q = 150$  kPa). The value of the earth pressure coefficient at rest was estimated as  $K_0 = 0.5$ . The amplitude of cyclic loading was kept constant at  $\Delta\sigma_1 = 60$  kPa in these tests. Initial relative densities of  $I_{D,0} = 0.29$  and  $I_{D,0} = 1.03$  were tested and compared with test No 3 whose average state of stress and cyclic amplitude were the same and whose initial relative density was determined as  $I_{D,0} = 0.58$ . The comparison of the results of these three tests can be found in Fig. 9. As could be expected the accumulated vertical and volumetric deformations were larger the lower the initial density was (see Figs. 9a) and 9b)). As can be seen from Figs. 9c) up to 9f) in all tests no significant changes of small strain properties could be observed. This was also true in the case of the loose

specimen which developed huge accumulated deformations and whose fabric should have changed strongly due to cyclic loading.

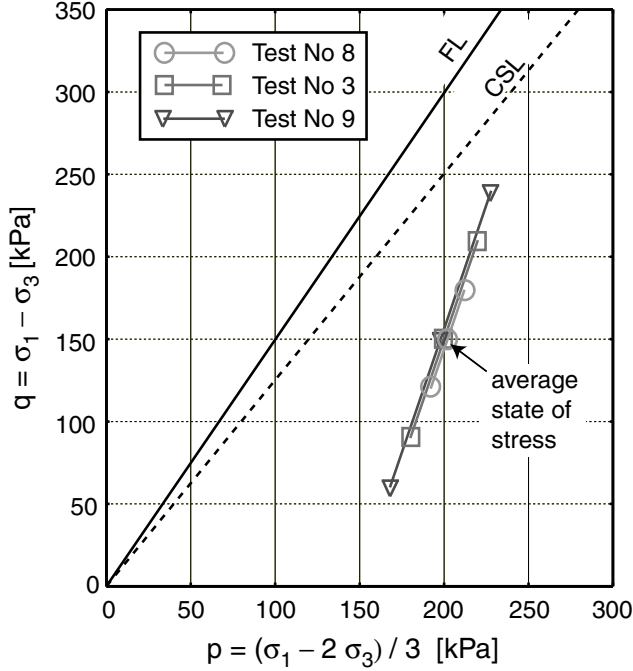


Fig. 10: Average state of stress and cyclic stress path in the cyclic triaxial tests with varying cyclic stress amplitude

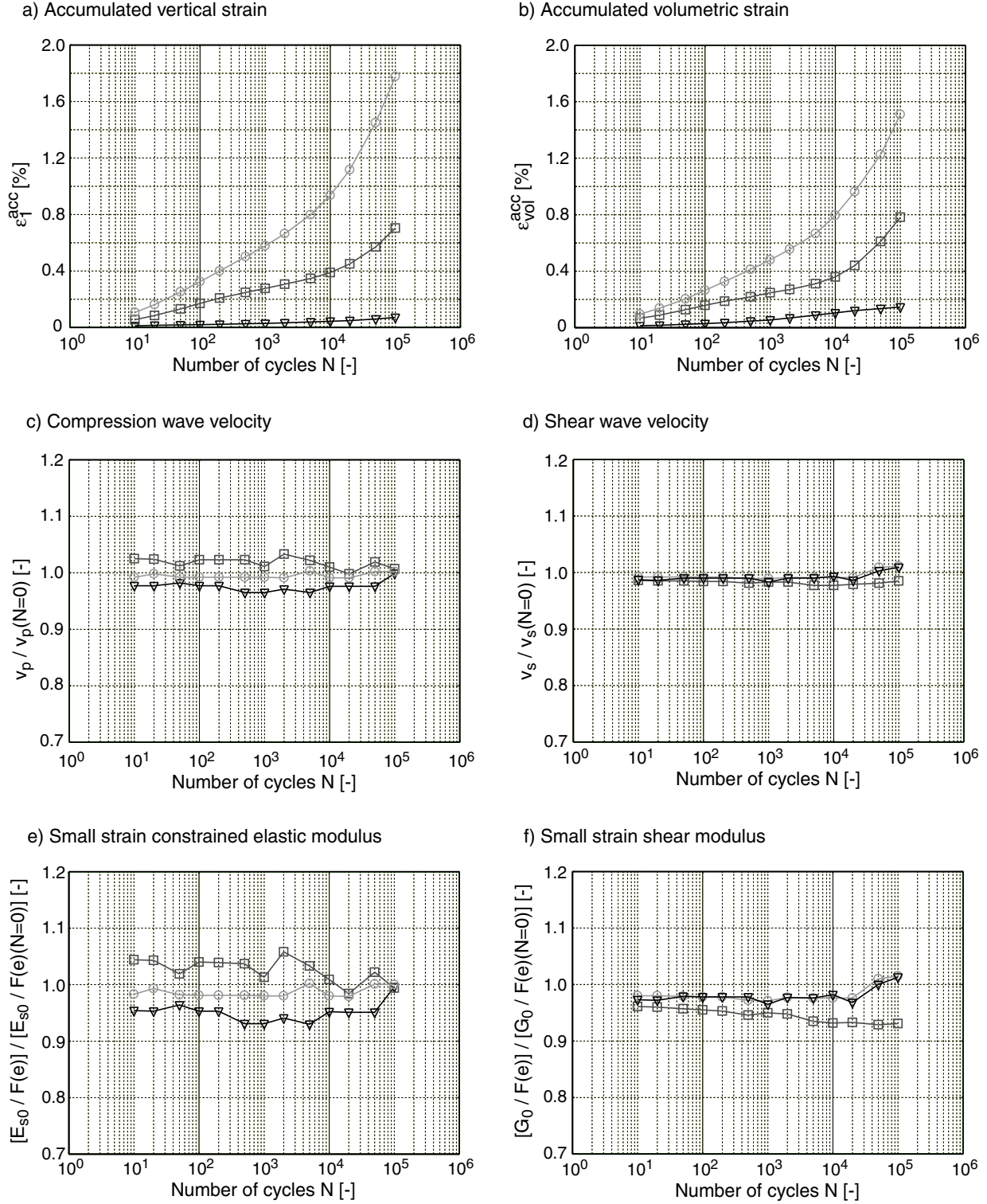
Tests No's 8 and 9 were conducted on medium sand 2 with varying amplitudes of cyclic loading resulting in different shear strain amplitudes as can be seen from Table 1. While test No 8 was performed with an amplitude of  $\Delta\sigma_1 = 30$  kPa, in test No 9 an alternating vertical stress of  $\Delta\sigma_1 = 90$  kPa was used. The tests were performed with an average state of stress lying on the  $K_0$ -line ( $p = 200$  kPa,  $q = 150$  kPa) and thus could be compared with test No 3 whose average state of stress was the same but which was performed with an amplitude of  $\Delta\sigma_1 = 60$  kPa. The maximum and minimum values of  $p$  and  $q$  in these three tests resulting from the average state of stress and the cyclic amplitude are presented in Fig. 10. Initial relative densities in these three tests lay in the range  $0.58 \leq I_{D,0} \leq 0.61$ . As can be seen from Figs. 11a) and 11b) the accumulated deformations increased with an increasing shear strain amplitude. Figs. 11c) up to 11f) indicate that although specimen fabric must have changed during cyclic loading only moderate changes of small strain shear moduli regardless the applied amplitude could be observed.

Fig. 12 contains signals received at different stages during test No 9. The determined arrival times of source and receiver signals are marked by the dashed vertical lines. It can be seen that the time difference between the source and receiver signal was not significantly affected by the cyclic loading. However, the

amplitude of the signals of bender elements and shear plates tended to decrease during the tests. The amplitude decay was stronger with increasing number of preloading cycles  $N$  applied to the specimen. For all the presentations in Fig. 12 the same amplification factor has been used. The results are indicating that this amplitude decay is caused by an increased material damping. The results for small strain excitations with the polarization perpendicular to the preloading direction indicates a significant change in material damping. It seems that the material damping is a more decisive factor among all the other small strain material properties for the indication of preloading history. For further justification of this statement more experiments will be needed.

In a last test the used sand was varied. Test No 10 was performed on fine sand. The specimen was prepared with an initial density of  $I_{D,0} = 0.50$  and was loaded cyclically with an average state of stress on the  $K_0$ -line ( $p = 200$  kPa,  $q = 150$  kPa) and an amplitude of  $\Delta\sigma_1 = 60$  kPa. Thus, this test could be compared with test No 3 whose average state of stress and cyclic stress amplitude were the same. The initial density of test No 3 was a little bit higher ( $I_{D,0} = 0.58$ ) than in test No 10. Nevertheless the generated shear strain amplitude due to the cyclic stress amplitude was lower in the case of the specimen of fine sand. The results are presented in Fig. 13. The medium sand generates larger accumulated deformations than the fine sand as can be seen from Figs. 13a) and 13b). This fact can partly be contributed to the different shear strain amplitudes in the two tests. Figs. 13c) up to 13f) indicate that wave velocities and small strain stiffnesses increased slightly and continuously during prestraining in the case of the fine sand while they stayed almost constant in the case of the medium sand. This stiffness increase of the fine sand did not exceed 10 % during 100,000 cycles in the curves of  $E_{s0}$  and  $G_0$ . These results coincide with data from resonant column tests with dynamic torsional prestraining of hollow cylinder specimens presented in [1] where the fine sand showed a slightly larger tendency of stiffness increase than the medium sand.

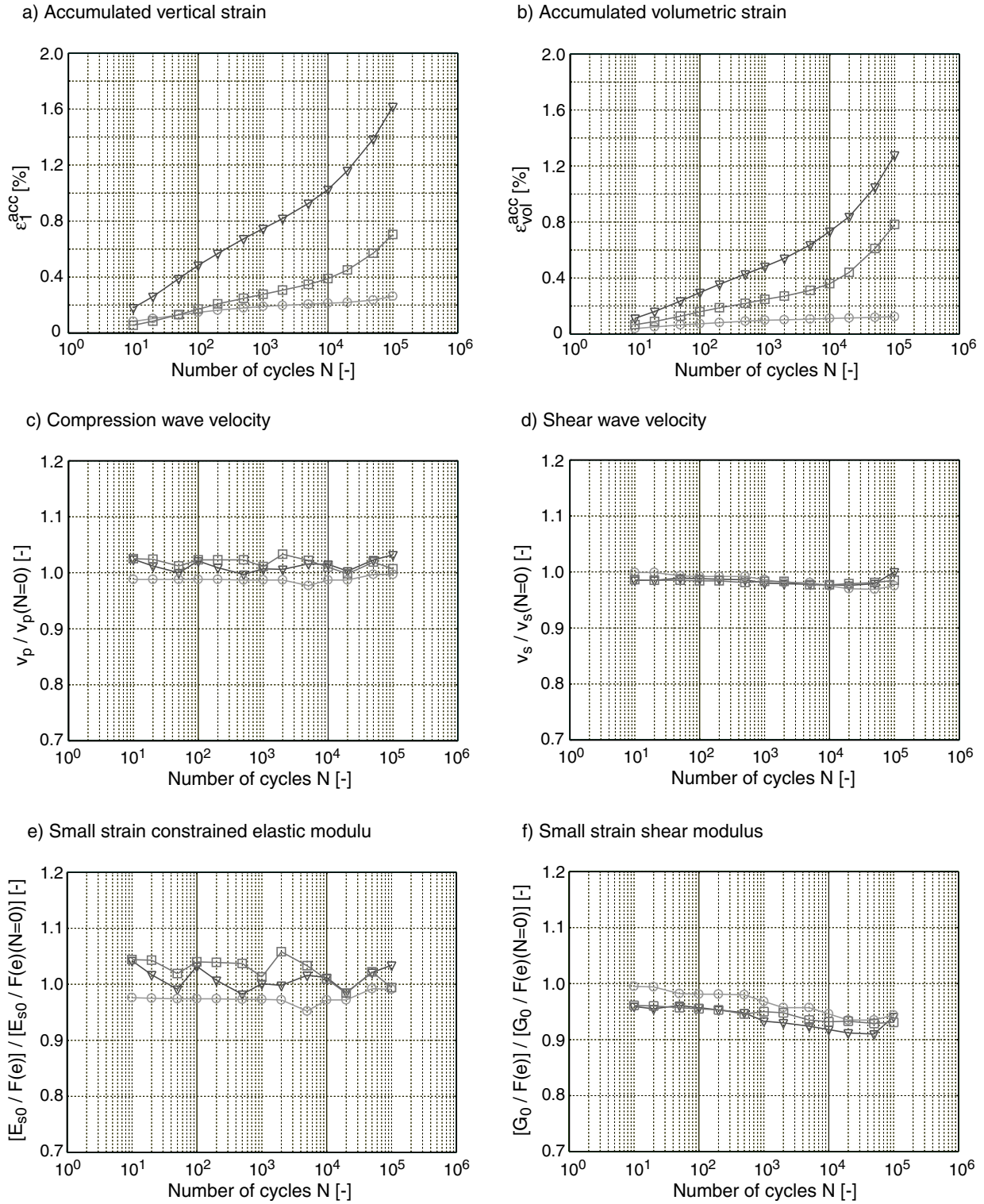
Fig. 14 summarizes small strain stiffnesses  $E_{s0}$  and  $G_0$  measured in the triaxial tests before the application of the first package of cycles. These values were obtained from tests with an anisotropic state of stress, i.e. the deviatoric component was not equal zero. The data of some tests not presented in the diagrams discussed above are added into Fig. 14. In Figs. 14a) and 14b) the measured values of  $E_{s0}$  and  $G_0$  are compared with values calculated by equations (5) and (7) with  $\sigma_a = \sigma_1$  and  $\sigma_p = \sigma_3$ , which are derived from tests with an isotropic state of stress. The curves obtained in the case of  $p = 200$  kPa and  $q = 100$  kPa, 150 kPa and 200 kPa did not differ very much so only one of



Legend for diagrams a) up to f):

○—○	Test No 6: $I_{D,0} = 0.29$ ; $I_{D,S} = 0.33$
□—□	Test No 3: $I_{D,0} = 0.58$ ; $I_{D,S} = 0.61$
▽—▽	Test No 7: $I_{D,0} = 1.03$ ; $I_{D,S} = 1.05$
all tests: $p = 200$ kPa, $q = 150$ kPa, $\Delta\sigma_1 = 60$ kPa	

Fig. 9: Results of cyclic triaxial tests with variation of initial relative density



Legend for diagrams a) up to f):

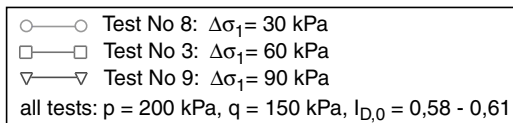
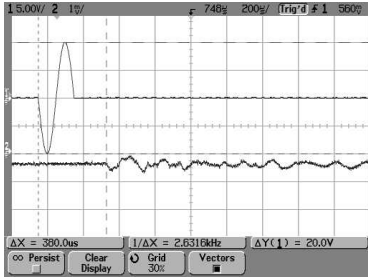


Fig. 11: Results of cyclic triaxial tests with variation of cyclic stress amplitude

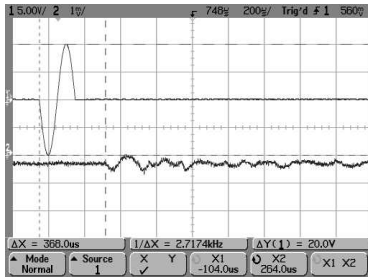
Test No 9,  $p = 200 \text{ kPa}$ ,  $q = 150 \text{ kPa}$ ,  $\Delta\sigma_1 = 90 \text{ kPa}$

Compression Element

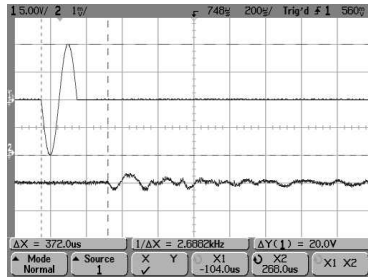
N = 0



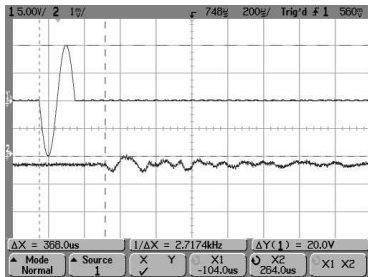
N = 100



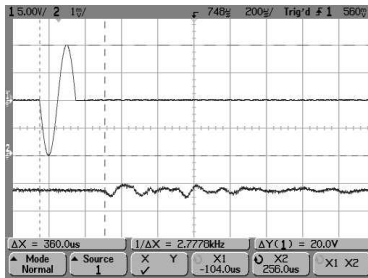
N = 1.000



N = 10.000

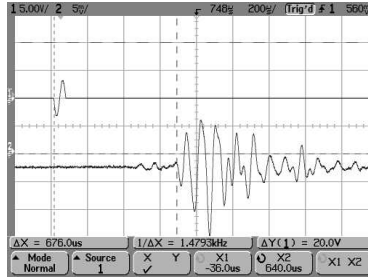


N = 100.000

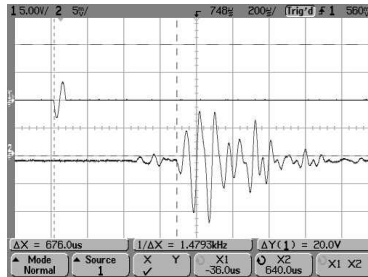


Bender Element

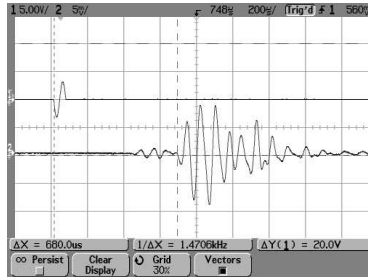
N = 0



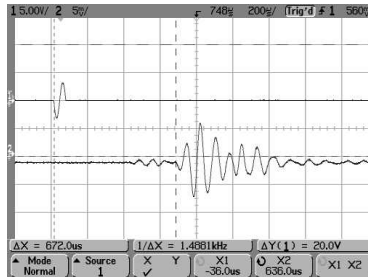
N = 100



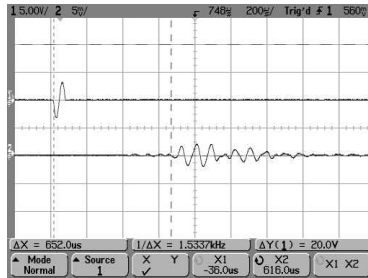
N = 1.000



N = 10.000

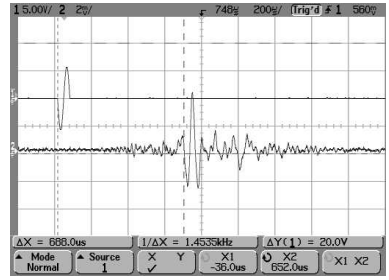


N = 100.000

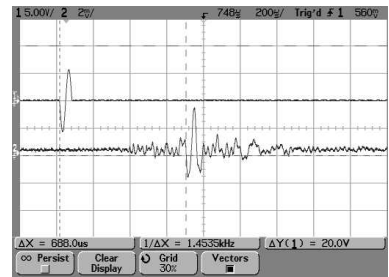


Shear Plate

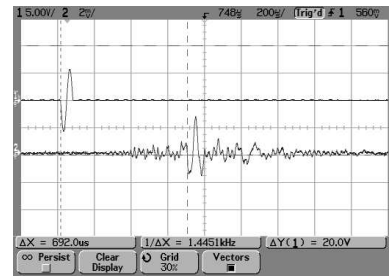
N = 0



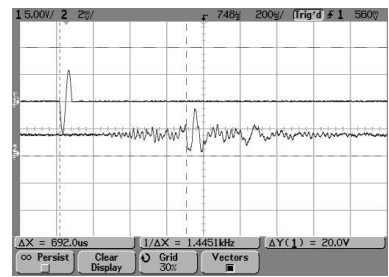
N = 100



N = 1.000



N = 10.000



N = 100.000

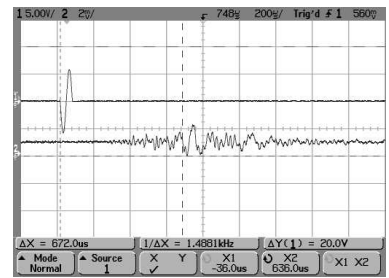


Fig. 12: Development of received signals in cyclic triaxial test No 9

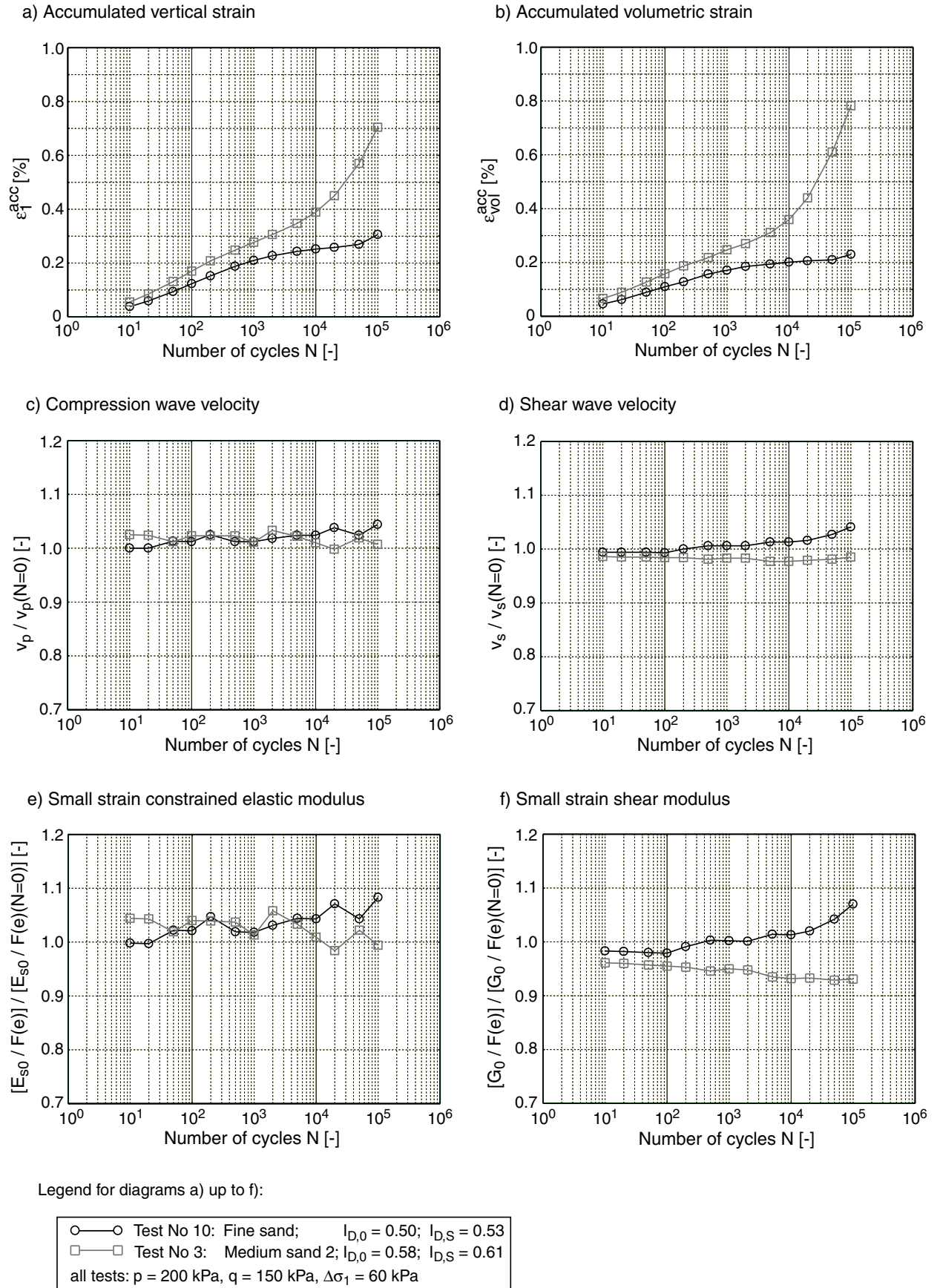
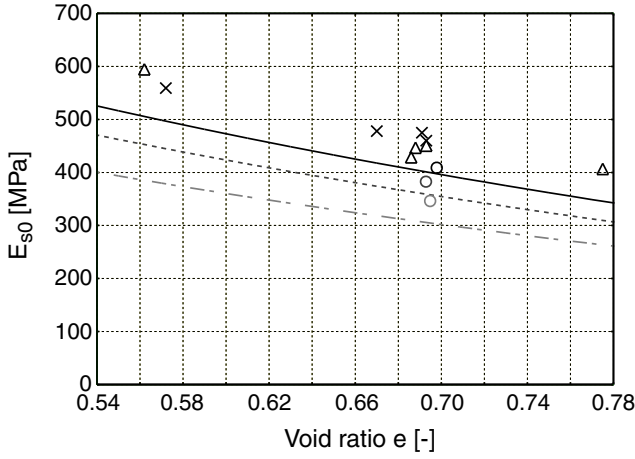
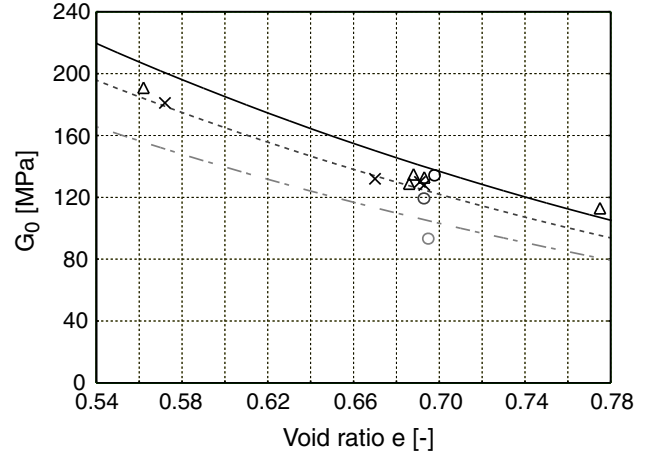


Fig. 13: Results of cyclic triaxial tests with variation of sand

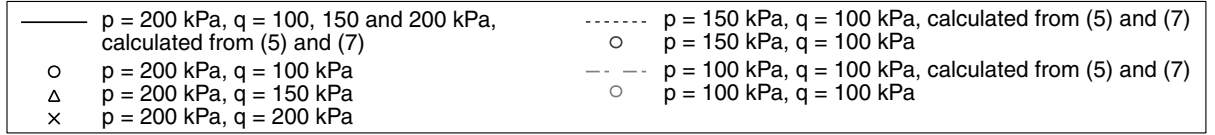
a) Small strain constrained elastic modulus



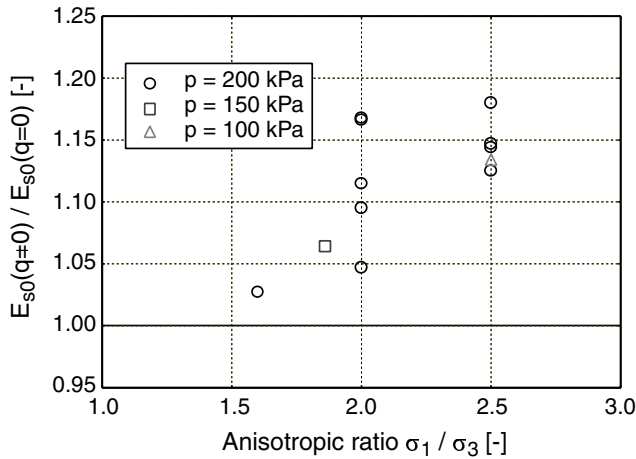
b) Small strain shear modulus



Legend for diagrams a) and b):



c) Percentual change of  $E_{s0}$  due to anisotropic stress



d) Percentual change of  $G_0$  due to anisotropic stress

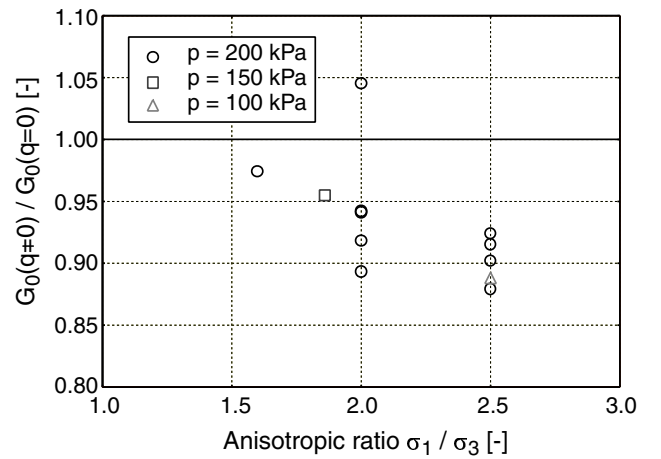


Fig. 14: Influence of an anisotropic state of stress on the small strain stiffnesses  $G_0$  and  $E_{s0}$

these curves is presented in Figs. 14a) and 14b). It can be seen from Fig. 14a) that the values of small strain constrained elastic modulus were increased due to the application of a deviatoric stress component. This increase was higher for higher  $q$  values. In Fig. 14c) the measured values of  $E_{s0}$  were related to values calculated from equation (5) using the respective void ratio of the specimen. The obtained normalized stiffnesses are presented as a function of the anisotropic ratio  $\sigma_1/\sigma_3$ . It can be clearly seen that the higher the anisotropic ratio was the higher was the increase of  $E_{s0}$  in comparison with the values determined in the case of an isotropic

state of stress. Small strain constrained elastic modulus  $E_{s0}$  could be increased up to nearly 20 % due to an anisotropic ratio of  $\sigma_1/\sigma_3 = 2.5$  in comparison with the values of  $\sigma_1/\sigma_3 = 1.0$  in the isotropic case. Fig. 14b) shows data for  $G_0$ . As can be seen the development of  $G_0$  due to the application of an anisotropic state of stress was opposite to that observed in the case of  $E_{s0}$ .  $G_0$  was reduced by the application of a deviatoric stress component. This fact was often reported in the literature (e.g. Yu and Richart [3]). As can be concluded from Fig. 14d) small strain shear modulus is reduced by approximately 10 % due to an applica-

tion of an anisotropic ratio of  $\sigma_1/\sigma_3 = 2.5$ . Similar values were obtained by Yu and Richart [3]. Considering Figs. 14a) and 14b) although the value of  $G_0$  of the loose specimen in test No 6 showed a somewhat scattering behaviour the dependence of the small strain stiffnesses on void ratio seems not to change significantly due to an anisotropic state of stress. It can be therefore concluded that the application of the void ratio functions (6) and (8) determined from tests with an isotropic state of stress is also valid in the case of the cyclic triaxial tests with an anisotropic average state of stress.

## 7 Summary and conclusions

The small strain stiffnesses measured in cyclic triaxial tests performed in this study did not show significant changes during 100,000 load cycles. This was found to be true independently of the chosen average state of stress, amplitude, relative density or sand. These moderate changes were observed although specimens partly showed huge accumulated deformations due to cyclic loading and thus the fabric of the specimens must have been changed. It has to be concluded that a change of fabric of specimens does not result in a significant change of small strain properties of dry sand. Thus, it is not possible to estimate the initial fabric or the preloading history, respectively of a sand by means of measurements of the small strain stiffnesses of the soil. This conclusion also resulted from the tests presented in [1] as well as from some test series presented in the literature which are also discussed in [1].

## Acknowledgements

This study was conducted as part of the subproject A8 "Influence of the fabric changes in soil on the lifetime of structures", which is supported by the German Research Council (DFG) within the scientific collaborative centre SFB 398 "Lifetime oriented design concepts". The authors are deeply indebted for this financial support, which is greatly acknowledged herewith.

## References

- [1] Wichtmann T, Triantafyllidis T. Influence of a cyclic and dynamic loading history on dynamic properties of dry sand, part I: cyclic and dynamic torsional pretraining. *Soil Dynamics and Earthquake Engineering* (submitted to publication)
- [2] Wichtmann T. Prognosis of densification potential of sand due to cyclic loading (in German). Diploma

thesis. Institute for Soil Mechanics and Foundation Engineering, Ruhr-University Bochum, December 2000

[3] Yu P, Richart F E. Stress ratio effects on shear modulus of dry sands. *Journal of Geotechnical Engineering*, ASCE, 1984; 110(3):331-345

[4] Bellotti R, Jamiolkowski M, Lo Presti D C F, O'Neill D A. Anisotropy of small strain stiffness in Ticino sand. *Géotechnique* 1996; 46(1):115-131

[5] Brignoli G M, Gotti M, Stokoe, K K II. Measurement of shear waves in laboratory specimens by means of piezoelectric transducers. *Geotechnical Testing Journal* 1996; 19(4): 384-397

[6] Wichtmann T, Sonntag T, Triantafyllidis T. On the memory capacity of sand under cyclic loading (in German). *Bautechnik* 2001; 78(12):852-865